Hot Methane Spectra for Astrophysical Applications

Christopher Andrew Beale

Submitted for the degree of

Master of Science
in
Physics

University of York

January 2012

Abstract

In this thesis line lists for methane (CH_4) are presented. These line lists were obtained at high temperatures (300-1400 ^oC at 100 ^oC intervals) by recording infrared emission spectra with a tube furnace to heat to the required temperatures and a Fourier transform spectrometer. The spectra were recorded in the range 800- 3400 cm^{-1} which includes the four fundamental modes; the bending modes that are composed of a pair of ν_2 (e) modes (at 1526 cm^{-1}) and a triply degenerate bending mode, ν_4 (a t_2 bend at 1306 cm^{-1}) and also the stretching modes that are

made up of a single symmetric ν_1 (a_1 at 2914 cm^{-1}) mode and a triply degenerate antisymmetric C-H stretch, ν_3 (a t_2 mode at 3020 cm^{-1}). The author analysed previously obtained data and recorded additional spectra at a higher wavenumber range (3000-7000 cm^{-1}). The analysis for this range has not yet been completed.

Empircal lower state energies are obtained from these spectra and these have been incorporated into the line lists. The line lists obtained from this work may be used to model the spectra of the atmospheres of exoplanets and brown dwarfs.

Table of Contents

List of Figures

Acknowledgements

I consider myself extremely fortunate to have been a member of the Bernath Group for a year. Firstly and most importantly I would like to thank Professor Peter Bernath for advising me for the duration of this thesis. To work with someone who is not only a distinguished scientist but also supports their students is a privilege. The students and post docs of the Bernath Group have been great company throughout my time there. Of particular note is Rob Hargreaves who advised me considerably through the rigmarole of the work associated with this thesis. His time, attention and effort (as well as data!) are greatly appreciated. Additionally, but no less importantly, I feel a great sense of appreciation for the Physics students at York, you allowed me down time, relaxation and frequent excursions into other labs. You all helped me through my 4 years at York and I'm a better person because of your company. Finally I would like to thank my family, particularly my parents who provided emotional and financial support throughout my time at York, without them I really would not have been able to do any of the things that I have been so lucky to have done. To everyone, thank you.

Author's Declaration

I confirm that this is my own work and the use of all material from other sources has been properly and fully acknowledged.

Christopher Beale

Substellar Objects

1.1 Introduction

1.1.1 Motivation

Molecular spectroscopy is an important diagnostic tool in atmospheric science. Spectra and lines assigned in the laboratory are frequently used in studying the atmospheres of planets and moons in our own Solar System (Courtin et al. 1984) those of extrasolar planets (Swain et al. 2009) as atmospheres of brown dwarfs. As knowledge of chemical spectra is a major limiting factor in the study of many objects in space (Fortman et al. 2010) it is important to take high resolution spectra in the laboratory in order to accurately analyze the spectra of these objects. Resulting line lists can be used to create model spectra for comparison with those obtained by observers. Brown dwarfs are described in detail in Section 1.2, and have been key spectroscopic targets in the infrared. Their relatively cool surface temperatures (<2000 K) of M-type stars and L-type brown dwarfs show the absorption bands of many metal hydrides, including CaH, CrH, LiH (Kirkpatrick 2005) and of more volatile gas species such as CH_4, H_2O, H_2 (Bernath 2009)

and NH_3 (Hargreaves et al. 2011). Many unassigned lines exist in the spectra of brown dwarfs. In order to assign these, currently line list data are extrapolated to pertinent temperatures as there are very few lists at the temperatures at which brown dwarfs exist (Hargreaves et al. 2011).

Extrasolar planets are planets that are in orbit around stars other than the Sun. Because of detection methods used, the known extrasolar planets are large and generally found in close orbit (<1 AU) around their parent star and are therefore usually hot gas giants. One class of very close orbiting (≤0.05 AU (Seager & Deming 2010)) extrasolar planets known as 'hot Jupiters' have long been thought to harbour atmospheres that may be detectable (Seager & Sasselov 1998). Transiting planets (a planet which passes in front of the star as seen from Earth) allow spectroscopic analyses of their atmospheres (Seager 2008; Bowler et al. 2010) with comparisons of observational data and theoretical models enabling the chemistry of the atmosphere to be examined. Since the first transiting extrasolar planet was discovered in 1999, (Charbonneau et al. 2000; Henry et al. 2000), 193 (as of December 21st 2011) have been found that orbit their parent star in this way. Spectroscopic study, either with space borne telescopes such as Spitzer or COROT, or ground based observations (Swain et al. 2010; Snellen 2008) of many of these planets is possible. Since the first exoplanetary atmosphere was observed in 2002, which found sodium features in the spectrum (Charbonneau 2002) dozens of such atmospheres have been observed (Seager & Deming 2010). Further observations in other planets have led to the detection of molecules such as H_2O, Na, CO, CO_2 and CH_4 (Tinetti et al. 2007; Redfield 2007; Swain et al. 2009) in their spectra. Indeed, with Earth sized planets being

discovered (Fressin et al. 2011) and the discovery of Keppler-20f being in the so called "habitable zone", i.e. a planet which orbits at the required radius and has the necessary atmospheric pressure to maintain liquid water, the possibility of finding an Earth twin is ever increasing. The study of exoplanets and brown dwarfs is therefore pertinent and study of their atmospheres (exoplanets in particular) can lead to the discovery of a planet that is Earth-like in the respect that life may be supported.

1.1.2 HITRAN and molecular line lists

In order for molecules to be assigned in spectra from astronomical sources, line lists for need to be archived in a database so that they may be accessed easily. One such database is the HIgh resolution TRANsmission (HITRAN) absorption database maintained at the Center for Astrophysics in Cambridge, MA. Spectroscopic parameters used as input for radiative-transfer codes may be obtained from HITRAN (Rothman et al. 2009) as well as the positions and intensities of the lines. Another major use of molecular spectroscopy is in studying our own atmosphere (Bernath 2009; Rothman et al. 2009). For this purpose, various lists of the intensity of the spectrum at a given wavelength are available. Given the temperature dependence of molecular transitions, different line lists exist for different applications.

This work is based off of the HITRAN (Rothman 2008) database which has been discussed in detail previously. NASA's Jet Propulsion Laboratory (JPL) provides line lists for transitions in the sub millimeter, millimeter and microwave (Pickett et al. 1998) which at these wavelengths are predominantly rotational transitions. These transitions at

low pressure are particularly useful for studying the interstellar medium. Other lists include The University of Denver Atlas of High-Resolution IR Stratospheric Spectra (Goldman et al. 1982) and GEISA (Gestion et Etude des Informations Spectroscopiques Atmosphériques: Management and Study of Spectroscopic Information) (Jacquinet-Husson et al. 2011)

Previous methane experiments to find methane absorption or emission data have been performed at low temperatures using cavity ring down spectroscopy (Wang et al. 2010a, 2010b; Campargue et al. 2010) and at high temperatures (Nassar & Bernath 2003). The low temperature (~80 K) line lists are particularly useful for studying planets and moons in our own solar system, notably Titan. However as will be discussed further, the temperature dependence of line intensity is important and as such low temperature lists are not adequate. A previous high temperature list (Nassar & Bernath 2003) provides line intensities from spectra at 800, 1000 and 1273 K at a resolution of 0.040 cm^{-1}) This type of line list is extremely useful for studying sub solar objects. However line intensities at more (higher, lower and more frequent) temperatures are needed, as such this body of work will produce line lists from 300-1400 ^{o}C at 100 ^{o}C intervals, at an increased resolution of 0.020 cm^{-1} and lower state energies of these transitions will be calculated which is additionally useful for theorists to calculate spectra for sub stellar objects. Therefore this thesis shows work which has improved upon previous measurements in a spectral region which is important for the transitions of methane and at temperatures which are relevant for astrophysical study.

1.2 Brown Dwarfs

Brown dwarfs may be simply classed as stars unable to fuse hydrogen into helium. The mass required for such fusion to occur is ~0.08 $M_{\odot}$ (Limber 1958) thereby defining an upper limit to the brown dwarf mass. With decreased mass, hydrostatic equilibrium, the point at which the gravitational collapse balances outward pressure, occurs at lower pressures and therefore lower temperatures than in hydrogen burning stars, with models predicting the brown dwarf interiors to have a maximum temperature of around $2x10^6$ K (Burrows et al. 2001), compared to $5x10^6$ K, the temperature required for hydrogen fusion. The temperature at which deuterium fuses is below that of hydrogen and is possible in brown dwarfs and it is the burning of deuterium which provides the low end requirement for the brown dwarf temperature regime, distinguishing them from extrasolar planets. Initially, most of the internal energy of a brown dwarf comes from its gravitational contraction and as there is little outward pressure from hydrogen fusion, the star will collapse until electron degeneracy pressure halts contraction and then it will cool thermally with no internal energy source. However, brown dwarfs are not fundamentally different from hydrogen burning stars. Both low mass stars and brown dwarfs have the same formation; it is only the amount of material available for accretion onto the young object that destines one to be a fully-fledged star and another to be a 'failed' brown dwarf star (Padoan & Nordlund 2004). Studies of stellar formation have found no major change in the spectra of protostars with mass to form an object either side of the 0.08 $M_{\odot}$ required for hydrogen burning (Luhman et al. 2003; Metchev 2005; Slesnick, Hillenbrand, & Carpenter 2004). They are therefore defined purely by the inability to fuse hydrogen.

1.3 Detection of Brown Dwarfs

First postulated in 1963 (Hayashi & Nakano 1963; Kumar 1963a, 1963b), initial searches for brown dwarfs involved looking for companions to main sequence stars. Identifying possible substellar objects is difficult against the brightness of the parent star, the intensity of which may be orders of magnitude greater than the target. The first confirmed brown dwarf was discovered as a companion to Gliese 229 (Oppenheimer et al. 1995), designated Gliese 229B. Since the early successes of searching for brown dwarfs as companions, wide sky surveys were commissioned to detect more as very few substellar objects were found using the direct imaging techniques used to find Gliese 229B.

The Two Micron All-Sky Survey (2MASS) (Gizis & Skrutskie 2001) was a study of the entire sky in the near infrared, based on two 1.3 m automated telescopes, one based at the Cerro Tololo Inter-American Observatory (CTIO), Chile and the other at Mt. Hopkins, Arizona. 2MASS is a collaboration between the Infrared Processing and Analysis Center (IPAC), who provided analysis of the data and the University of Massachusetts which assumed overall responsible for management of the survey. Part of the remit for the survey was to observe cool objects that are more easily observed in the infrared such as brown dwarfs and other low luminosity stars. 2MASS images the entire sky in the near infrared at J (1.25 μm), H (1.65 μm) and K_S (2.17 μm) simultaneously (Burgasser et al. 2002; Burgasser et al. 2003) in order to distinguish cool objects from their hot parent stars.

DENIS, the DEep Near-Infrared Survey (Epchtein 1998), was a consortium using a 1 m telescope at the European Southern Observatory (ESO) at La Silla, Chile to image the sky at 0.8 μm, 1.25 μm and 2.16 μm running from 1996 to 2001. DENIS operates at the optical colour band I (0.82 μm) and the infrared colour bands J (1.25 μm) and K_S (2.17 μm).

Gliese 229B has a temperature of 950±80 K (Geissler, Chauvin, & Sterzik 2008; Saumon et al. 2000) and is typical of the temperatures of a T-type dwarf. Figure 1.1: Observed near-infrared spectra of 2MASS 0415-09 (Knapp et al. 2004), 2MASS 0939-24 and 2MASS 1114-26 (Burgasser et al. 2006) showing the flux at different wavelengths with molecules assigned. (Leggett at al. 2007)

Figure 1.1 shows the similarity in spectra between three T-type dwarfs. The importance of laboratory measurements in this region is highlighted in Bernath (2009) with water, methane and ammonia being present in these low temperature type dwarfs, (higher temperature M-type dwarfs having metal oxides in their atmospheres (Burrows et al. 2005) and laboratory spectra have been used in this temperature regime by Cushing et al. (2005). Figure 1.1 shows some of the molecules are spectrally active in the infrared. Previously, this chapter has mentioned the metal hydrides and metal oxides as well as gases such as methane, ammonia and water vapour. Clearly infrared spectra of brown dwarfs are highly active in various molecules of interest that can help observers determine the conditions of such objects.

Through astronomical observation, distinction between a large planet and a small star is not an easy one; studies of WD 0137-349B for example have not been definitive in a

classification (Burleigh et al. 2006). Indeed the need for more infrared spectroscopy to determine the nature of substellar objects is especially important for brown dwarfs, which may be considered 'in between' (in nature) planets and stars. Their characteristics may be determined by spectroscopy of the object in the infrared. Indeed, in order to ascertain the spectral type and luminosity, varying photometric measurements and infrared spectroscopy are required for brown dwarfs in binary systems, due to asymmetric heating of the brown dwarf (Maxted et al. 2006). The temperature of the star is a property of the spectral type, and therefore measurement of the varying temperature throughout the orbit of one binary partner around the other can yield information about both stars.

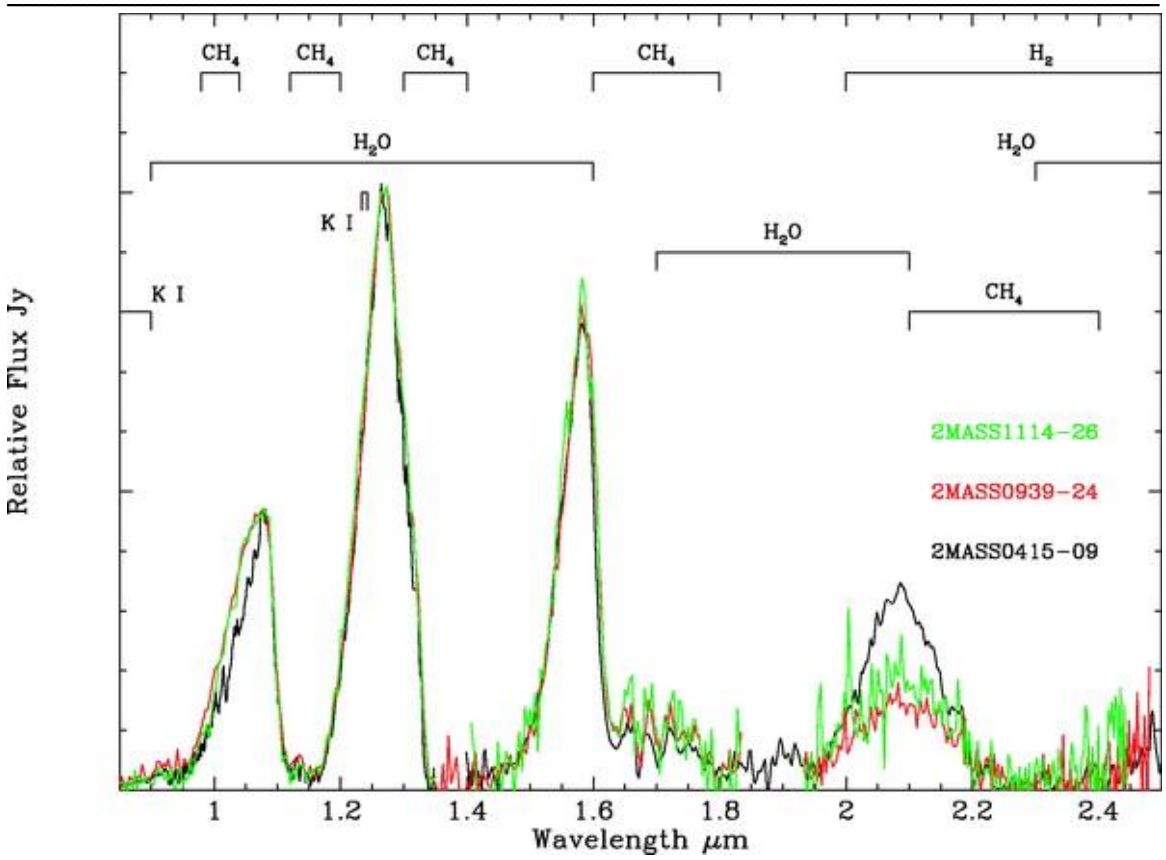

Figure 1.1: **Observed near-infrared spectra of 2MASS 0415-09 (Knapp et al. 2004), 2MASS 0939-24 and 2MASS 1114-26 (Burgasser et al. 2006) showing the flux at different wavelengths with molecules assigned. (Leggett at al. 2007)**

1.4 Extrasolar Planets

Planets are ubiquitous objects in astronomy, studies of the planets of our solar system have been ongoing for centuries. However, the observation of planetary atmospheres began in the 1920s (Seager & Deming ; Webster 1927) giving rise to the idea that the

chemistry and physics of planets are not necessarily the same as Earth's. The existence of planets around other stars was a logical prediction and in 1995 the first confirmed extrasolar planet was found orbiting around the star 51 Pegasi (Mayor & Queloz 1995). 51 Peg b is not like any planet in our solar system, although it has mass on the scale of Jupiter (0.472 M_J), its orbit is 0.05 AU from the parent star and therefore has an extremely hot surface temperature for a planet (~1300 K). This temperature regime is fairly typical of exoplanets, although there is little physical reason why this should be the case given that the science of planetary formation is not well understood. However, this range of temperatures provides an energy distribution with which it is possible to observe transitions of methane, ammonia and water. Since most stellar surfaces are generally too hot to sustain these molecules without dissociation, a spectrum containing these compounds is indicative of a cool surface.

The detection bias of extrasolar planets, which will be outlined in the following sections, means that those planets that we know of are typically very large or have close orbits to their parent star. Figure 1.2 shows the variance of planetary mass against the orbital radius, the detection bias of both methods is given in 1.4 and is shown clearly in Figure 1.2. The detection and study of extrasolar planets is of interest because of the possible discovery of a planet that may harbour habitable conditions for life forms. The challenge then is not only in discovering a small planet in the so called "Goldilocks Zone", that is to say the temperature is not too hot and not too cold for life to exist, but also a spectroscopic challenge of whether or not these planets have atmospheres in which life can flourish.

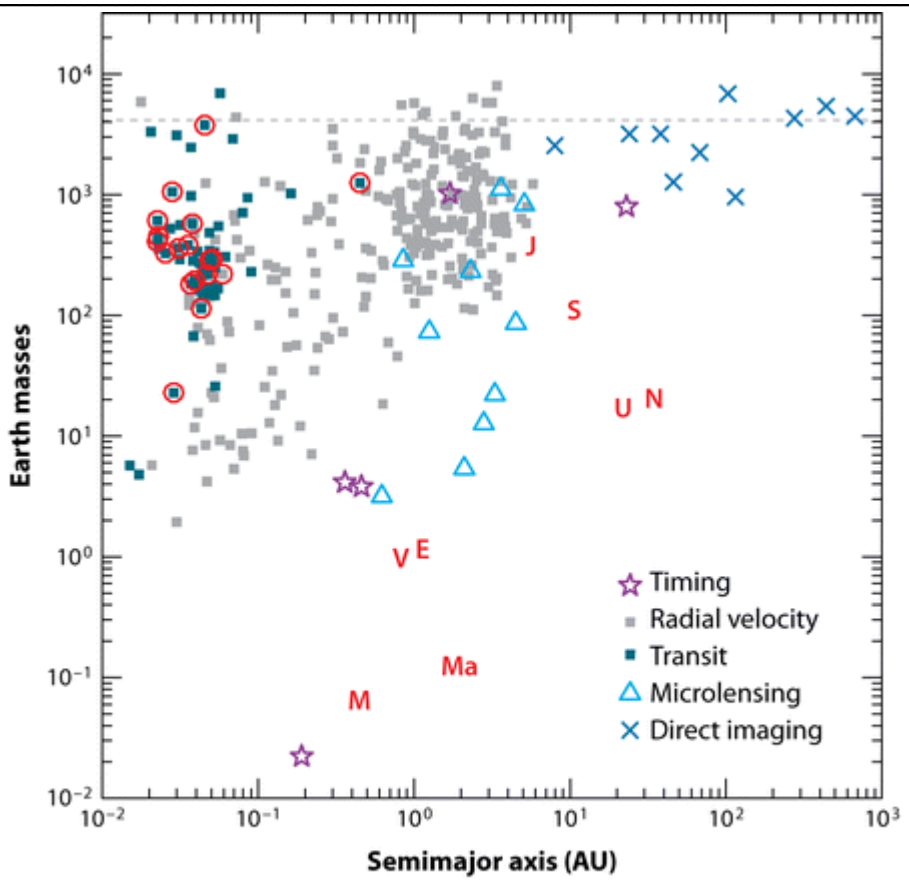

Figure 1.2: **Various exoplanets plotted by detection technique showing the dependency of detection on mass or proximity to the star (Seager & Deming 2010)**

1.5 Detection of Exoplanets

Of the hundreds of exoplanets known (http://exoplanets.eu/) the majority were discovered by using one of two methods; the radial velocity method and the transit method (see Figure 1.2).

The radial velocity technique is to date the most successful method for detecting exoplanets and arrives from the fact that a planetary system will orbit around its centre of mass. The star is therefore rotating, appearing to move backwards and forwards to the observer on Earth and the light from the star will be periodically Doppler shifted, red shifted when the star moves away from the observer and blue shifted when it moves towards them. Fundamental and well defined atomic or molecular absorption lines in the spectrum of the star that are detected on Earth will also be shifted (Baranne et al. 1996). By measuring the radial velocity of the star of mass M_* and knowing its orbit around the centre of mass, we can obtain both the orbital period, P of the planet and its eccentricity, e. The product of the mass, M_p and the orbital inclination, i of the planet is given by the equation for the semi amplitude radial velocity (K) equation

$$K = \left(\frac{2\pi G}{P}\right)^{1/3} \frac{M_p \sin i}{\left(M_* + M_p\right)^{2/3}} \frac{1}{\sqrt{1-e^2}} \qquad [1]$$

the parameter K can be obtained from the radial velocity graph (see Figure 1.3). However, since the inclination is not directly measurable, the mass of the planet is a minimum and requires additional methods of measurement to be accurately determined. Since the identification of an object as a planet or brown dwarf companion is based on mass, the radial velocity method despite being a powerful detection technique method is not as quantitative as other methods such as the transit method.

The technique is more sensitive to planets of higher mass (Bernath 2009) and which orbit their parent stars at a short distance. Such planets are called ‘hot Jupiters’ due to their atmospheric temperatures and masses on the Jovian scale. The radial velocity method

also clearly favours planets that are in our radial plane of view (that is to say 'side on' where the orbital inclination is approximately 0°) as opposed to planets which orbit normal to our plane of view therefore having no radial motion and whose detected spectral lines are not Doppler shifted. Although the actual mass remains ambiguous, most exoplanets orbit around their star in our line of sight (Santos2008) approximating sin *i* to 1 (Jorissen et al. 2001) so the estimate for the minimum mass is likely to be similar to the actual mass.

The first discoveries of exoplanets orbiting Sun-like stars were done so using the radial velocity technique including 51 Pegasi b (Mayor & Queloz 1995; Marcy et al. 1997), 47 Ursa Majoris b Butler & Marcy 1996) and Gliese 876 b (Marcy et al. 1998). Although since the discovery of 51 Peg b, which has a radial velocity variation of around 60 ms^{-1} (see Fig. 1.3), new spectrographs such as HARPS (High Accuracy Radial planet Searcher) can detect variations of as low as 1 ms^{-1} (Pepe et al. 2003; Baraffe et al. 2003). With more powerful spectrographs come more problems. Stars are not isotropic entities (Thorne & Campolat 1967) and in time stellar fluctuations can cause a change in the radial velocity similar to that of the gravitational effect of a small planet (Saar & Donahue 1997; Creevey et al. 2010).

Overall, the radial velocity technique is an extremely powerful method for exoplanet discovery and gives a relatively good estimation for the mass of the planet and some information regarding its orbit. However to more fully understand the properties of an exoplanet, other measurement techniques are required.

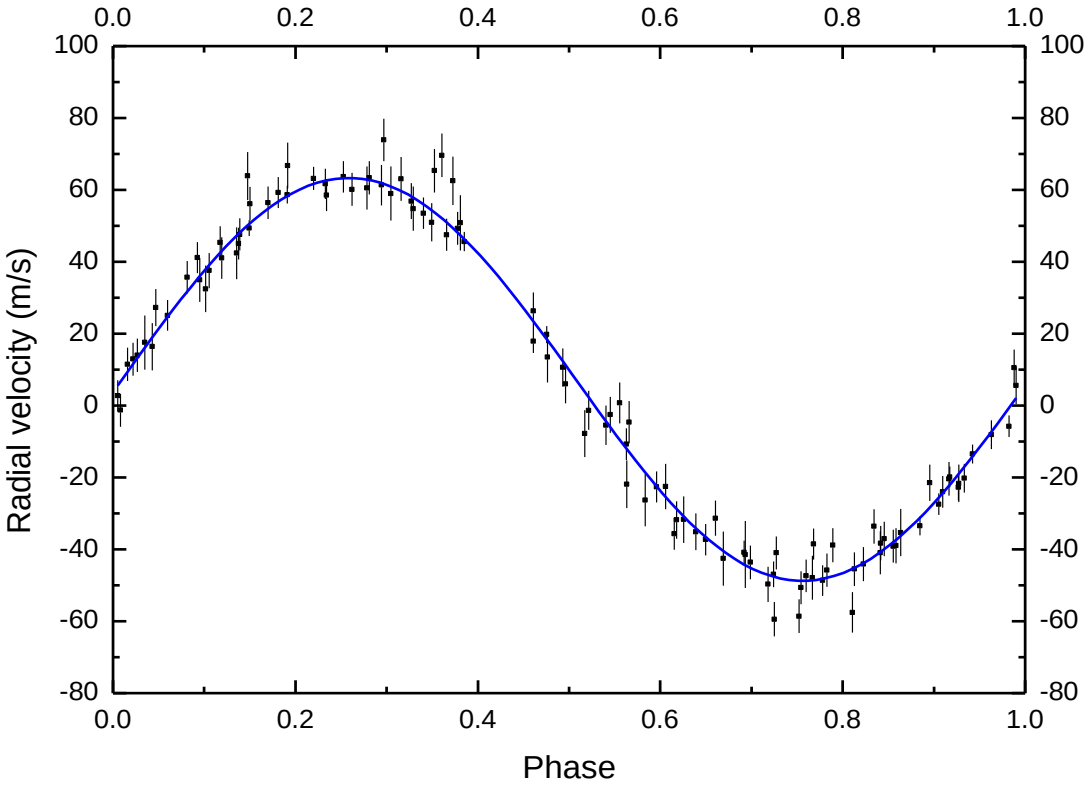

Figure 1.3: Radial velocity curve with a Keplerian fit of 51 Peg. Data from Marcy et al. (1997) over 324 days, reduced here to 1 phase (4.230 days).

When looking from Earth, an object may pass between the observer and a source of light. In astronomy, a cosmic source of light is most frequently a star and if an orbiting planet is the transiting object we may be able to detect it. The so-called transiting technique is different from the radial velocity method in that it is photometric, that is to say it measures the luminosity of the star. Much in the same way as an object passing between us and our Sun, an orbiting exoplanet passing through our line of sight to its parent star

will block light from that star, and depending on the light curve that results from photometric observations, the presence of a planet may be detected and atmospheric properties may be inferred. Indeed, most current knowledge of physical characteristics (interior temperature, atmospheric composition and density) of exoplanets have resulted from studies of exoplanet transits (Seager 2008) and is therefore a hugely important part of exoplanetary study.

To be detectable on Earth, the transit must be approximately perpendicular to our line of sight. The probability P for this to occur for a planet circularly (which can be assumed to be approximately correct since the planet is transiting) orbiting a star of radius R_* at a distance a is given by

$$P = \frac{R_*}{a} \qquad [2]$$

And for most hot Jupiters (a = 0.5 AU) this results in a P ~ 10%. However, for a planet at 1 AU, this probability is reduced to ~0.5% and for a planet at 5 AU (roughly the orbit of Jupiter) the probability is ~0.1%. Clearly, unlike the radial velocity of a star which is caused by the mass of the planet, the photometric variations as seen in Fig. 2.4 are caused by the area of the disk that blocks the starlight out and to a lesser extent the translucency of any atmosphere the planet may have.

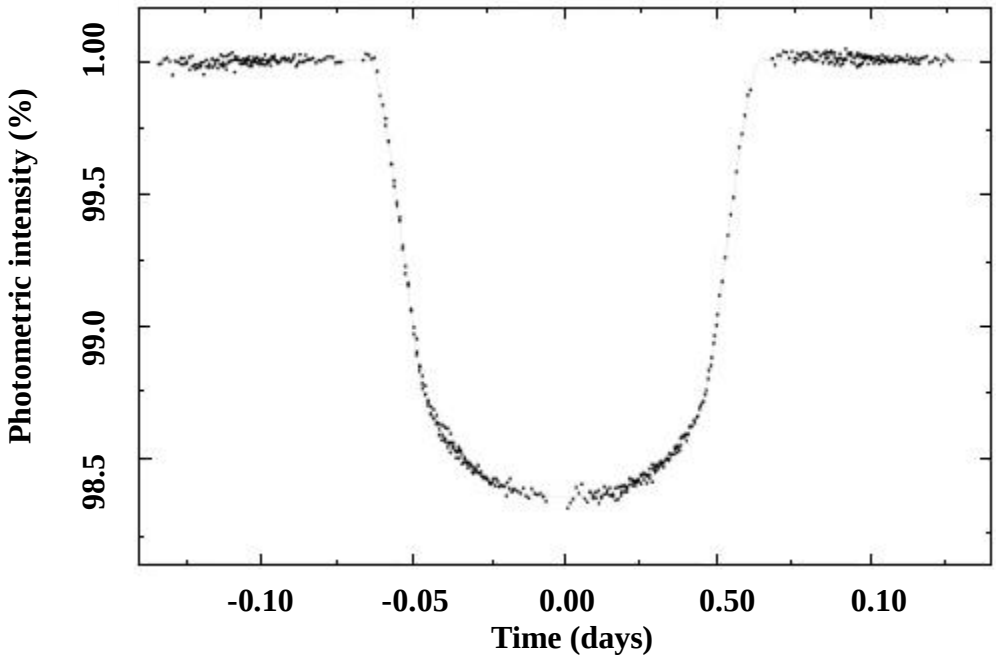

Figure 1.4: Hubble Space Telescope photometry of the star HD 209458, the drop in light intensity suggests a radius of the exoplanet, named HD 209458b, to be approximately 1.35 Jupiter masses (M_J) From Brown et al. (2001).

And the orbital period t is then given, presuming an equatorial transit (Santos 2008), by,

$$t = \frac{R_* P}{a\pi} \qquad [3]$$

for observational purposes it preferable to observe short period orbits as determination of the existence of an orbiting body from a luminosity change from a light curve depends on a regular and consistent decrease in light from the star to be measured.

Given that the star and planet are both assumed to be uniform disks, the light curve yields the decrease in luminosity, ΔL as a function of the size of the discs;

$$\Delta L = \left(\frac{R_p}{R_*}\right)^2 \quad [4]$$

Mass determination is more difficult however. Seager and Mallén-Ornelas (2003) show how parameters for the system (R_*, M_*, $R_!$, a and i) can be derived from the light curve and this leads to an estimation of the mass in combination with radial velocity measurements (Santos 2008; Tuomi et al. 2009).

The photometric signal, such as that which may be seen from an exoplanet, is not indicative of one. An orbiting body such as a low mass brown dwarf creates a flux change indistinguishable from that of a large Jovian planet (Pont et al. 2005a). Beyond the simple Sun-like star and low orbit hot Jupiter system that only accounts for a minority of solar systems, there are multiple star systems, including M dwarfs orbiting giant single stars or multiple blended star signals (Santos 2008) that give similar flux decreases to exoplanetary systems (Bouchy et al. 2005; Pont et al. 2005b). As such, to both detect an exoplanet and to determine the physical characteristics of it as listed above, both methods must be used in unison.

However, as has been discussed, the probability of observing a transit in a given system is around 10% or less and therefore for the majority of exoplanets, we are unable to know more about the planet than its mere existence. Notwithstanding this fact, transiting

exoplanets provide a useful passive spectroscopic system. The spectrum of the star on its own and the spectrum of the star and planet in front of it can yield a spectrum showing the chemical composition of that planet. Indeed, this technique was used to first discover methane in the atmosphere of an exoplanet (Swain et al. 2008) a brown dwarf (Oppenheimer 1995). In addition to observing methane in the atmospheres of sub stellar objects, the absorption or emission features of key molecules in the spectrum, such as water (Oppenheimer 1995) can yield measurements for the calculation of the atmospheric temperature.

References:

Baraffe, I., et al., 2003, Astronomy & Astrophysics, 402(2) 701

Baranne, A., et al., 1996, Astronomy & Astro. Sup. Series, 119(2) 373

Bernath, P. 2009, International Reviews in Physical Chemistry, 28, 681

Bouchy, F., et al. 2005, Astronomy & Astrophysics, 431(3), 1105

Burgasser, A. J., et al. 2002, Astrophysical Journal, 564, 421

Burgasser, A. J., et al. 2003, Astronomical Journal, 125, 850

Burleigh, M. R., et al. 2006, MNRAS, 373, L55

Brown, T.M., et al., 2001, Astrophysical Journal, 552(2), 699

Burrows, A., Hubbard, W. B., Lunine, J. I., & Liebert, J. 2001, Reviews of Modern Physics, 73, 719

Butler, R. P., & Marcy, G. W. 1996, Astrophysical Journal, 464, L153

Campargue, A., et al. 2010, JQSRT, 111, 1141

Creevey, O.L., et al., 2010, Astronomische Nachrichten, 331(9-10, 952

Epchtein, N. 1998, in New Horizons from Multi-Wavelength Sky Surveys, eds. B. J. McLean, D. A. Golombek, J. J. E. Hayes, & H. E. Payne (Dordrecht: Kluwer Academic Publ), 106

Geissler, K., Chauvin, G., & Sterzik, M. F. 2008, Astronomy & Astrophysics, 480, 193

Gizis, J. E., & Skrutskie, M. F. 2001, in Extragalactic Infrared Background and Its Cosmological Implications, eds. M. Harwit, & M. G. Hauser (San Francisco: Astronomical Soc Pacific), 197

Goldman A. et al. 1982, Applied Optics, 21, 1163

Hargreaves, R. J. et al. 2011, Astrophysical Journal, 735, 111

Hayashi, C., & Nakano, T. 1963, Progress of Theoretical Physics, 30, 460

Jacquinet-Husson, N. et al. 2011, JQSRT, 112, 2395

Jorissen, A. Mayor, M & Udry. S. 2001, Astronomy & Astrophysics, 379(3), 992

Kirkpatrick, J. D., 2005, ARA&A, 43, 195

Kumar, S. S,. 1963a, Astrophysical Journal, 137, 1126

Kumar, S. S., 1963b, Astrophysical Journal, 137, 1121

Leggett, S. K., et al., Astrophysical Journal, 710, 1627

Limber, D. N. 1958, Astrophysical Journal, 127, 387

Luhman, K. L., et al. 2003, Astrophysical Journal, 593, 1093

Marcy, G. W., Butler, R. P., Vogt, S. S., Fischer, D., & Lissauer, J. J. 1998, Astrophysical Journal, 505, L147

Marcy, G. W., et al. 1997, Astrophysical Journal, 481, 926

Maxted, P. F. et al., 2006, Nature, 422, 543

Mayor, M., & Queloz, D., 1995, Nature, 378, 355

Metchev, S. A. 2005, PhD thesis (Pasadena: California Institute of Technology)

Nassar, R. & Bernath, P. F., 2003, JQSRT, 82, 279

Oppenheimer, B. R., et al. 1995, Science, 270, 1478

Padoan, P., & Nordlund, A., 2004, Astrophysical Journal, 617, 559

Pepe, F., et al., 2003, Scientific Frontiers in Research on Extrasolar Planets, D. Deming and S. Seager, Editors. Astronomical Soc Pacific: San Francisco. p. 39- 42.

Pickett, H. M., et al., 1998, JQSRT, 60, 883

Pont, F., et al., 2005a, Astronomy & Astrophysics, 433(2), L21

Pont, F., et al., 2005b, Astronomy & Astrophysics, 438(3), 1123

Saar, S.H. & R.A. Donahue, R.A., 1997, Astrophysical Journal, 485(1), 319

Santos, N.C., 2008, New Astronomy Reviews, 52(2-5), 154

Saumon, D., et al., 2000, Astrophysical Journal, 541, 374

Seager, S. & Mallen-Ornelas, G., 2003, Scientific Frontiers in Research on Extrasolar Planets, D. Deming & S. Seager, Editors, Astronomical Soc. Pacific: San Francisco. 419

Seager, S., 2008, Space Science Reviews, 135(1-4) 345

Seager, S. & Deming, D., 2010, Annual Review of Astronomy and Astrophysics, Vol 48 (Palo Alto: Annual Reviews), 631

Slesnick, C. L., Hillenbrand, L. A., & Carpenter, J. M., 2004, Astrophysical Journal, 610, 1045

Thorne, K.S. & Campolattaro A., 1967, Astrophysical Journal, 149, 591

Tuomi, M., Kotiranta, S. & Kaasalainen, M., 2009, Astronomy & Astrophysics, 494(2), 769

Wang, L., Kassi, S., Campargue, A., 2010a, JQSRT 111, 1130

Wang, L., et al 2010b J. Mol. Spectrosc. 261, 41

Webster, D. L., 1927, Nature, 120, 879

Chapter 2

An Introduction to Infrared Spectroscopy

2.1 Vibrational Spectroscopy

The three dimensional Schrödinger equation of the system of N particles is described as (Herzberg 1991)

$$\sum_i \frac{1}{m_i}\left(\frac{\partial^2\psi}{\partial x_i^2}+\frac{\partial^2\psi}{\partial y_i^2}+\frac{\partial^2\psi}{\partial z_i^2}\right)+\frac{8\pi^2}{h^2}(E-V)\psi=0 \qquad [5]$$

where *m* is the mass of a particle, E the total energy and V the potential energy. In a diatomic molecule, the bond can be modelled by a spring between two point masses. The vibration is then described with simple harmonic motion (SHO). The eigenvalues for the resulting one dimensional SHO are given by (Rae 2002)

$$E = E_n = \hbar\omega_c\left(v+\frac{1}{2}\right) \qquad [6]$$

where $\omega_!$ is the angular frequency at which the potential is oscillating and v is the vibrational quantum number. The resulting energy levels will be equally spaced at intervals of

$$E = \hbar\sqrt{\frac{K}{\mu}}\left(v + \frac{1}{2}\right) \quad [7]$$

where K is the spring constant and μ is the reduced mass of the system. In the applied system of a chemical bond, the spring constant is determined by the strength of the bond between the two atoms. In a physical system, i.e. one involving actual molecules, due to the finite energy levels and eventual dissociation of the molecule at a certain energy levels, the potential has cubic and other anharmonic terms. These *eigenvalues* (vibrational energy levels) are collected and describe the vibrational energy of the system as follows

$$G(v) = \omega_k\left(v_k + \frac{1}{2}\right)^2 + \omega_k\left(v_k + \frac{1}{2}\right)^2 + \omega_k\left(v_k + \frac{1}{2}\right)^3 + \cdots \quad [8]$$

Each constituent atom has three degrees of freedom, one in each spatial coordinate. A molecule containing N atoms will therefore have 3N degrees of freedom. For the molecule as a whole however, there are three translational modes and a rotational mode about each axis. For a three dimensional molecule there are three such rotational modes. As such there are a total of 3N – 6 degrees of freedom.

The total vibrational energy of the system is therefore

$$\sum_{k}^{3N-6} \hbar\omega_k \left(v_k + \frac{1}{2}\right) \quad [9]$$

The 3N – 6 modes of the methane molecule are made up of four stretching modes and five bending modes (Bernath 2005). These nine modes may be reduced to four frequencies (Figure 2.1). A symmetric stretch, v_1 shown in A, a triply degenerate antisymmetric stretch, v_3 shown in C, a pair of e mode bends, v_2 in B, and a triply degenerate bend, v_4 in D.

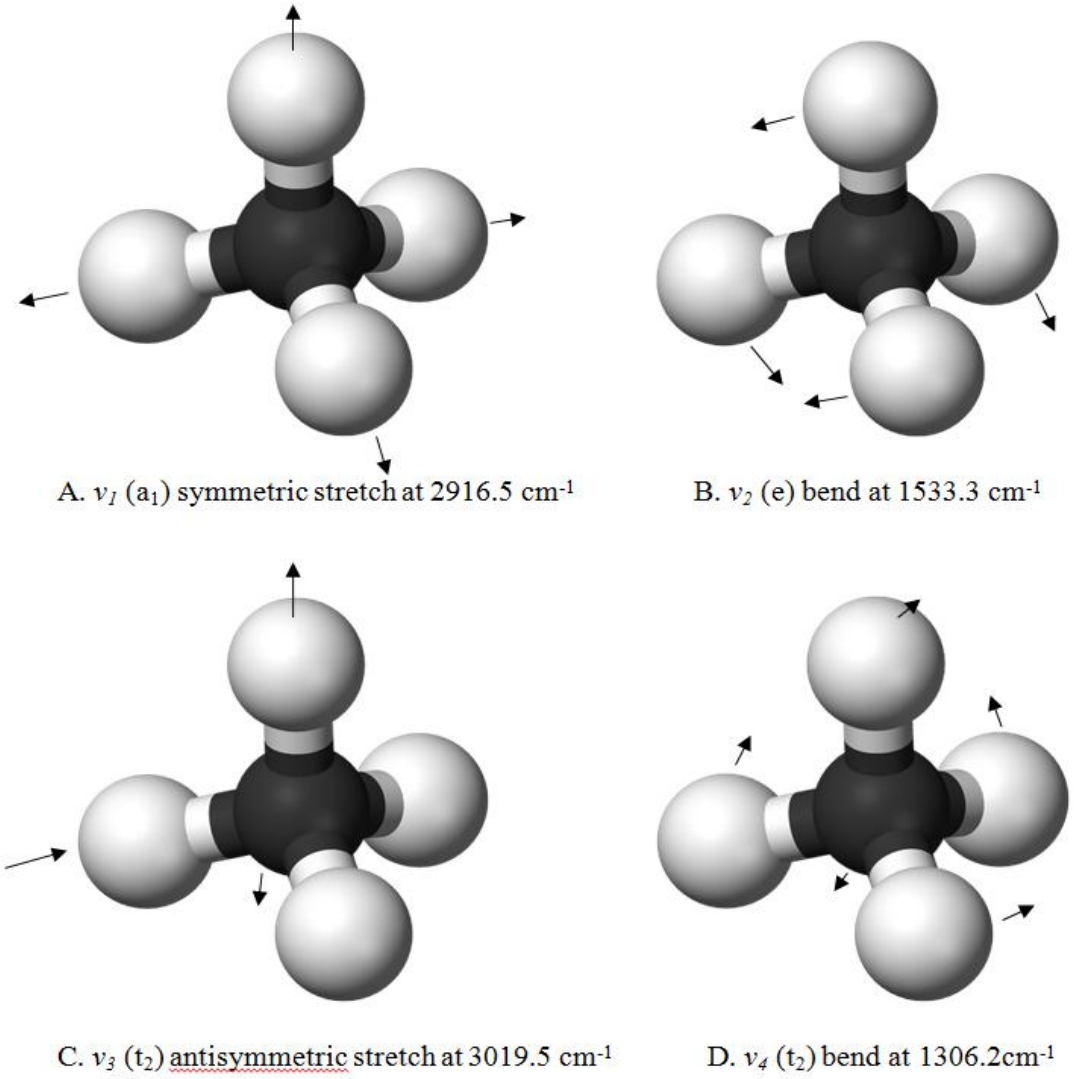

Figure 2.1: A schematic representation of the four reduced fundamental vibrational modes of methane, the band centres stated are given by Herzberg (1991).

2.2 Rotational Spectroscopy

Rotational spectra arise from changes in the angular momentum of a molecule. In any three dimensional object, such as a molecule, there are three independent axes that are mutually perpendicular to each other, I_A, I_B and I_C.

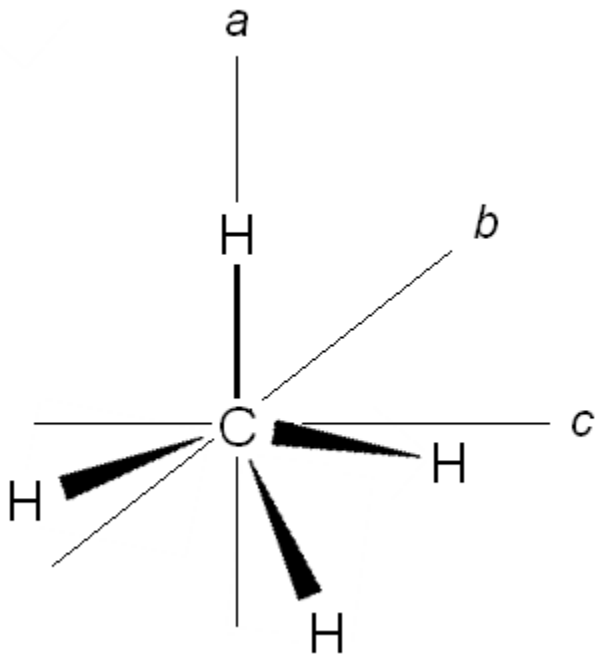

Figure 2.2: A schematic of the independent axes of the spherical rotor, methane.

The moment of inertia about each axis is given by

$$I = \sum_i m_i \rho_i^2 \qquad [10]$$

Where m_i is the mass of each atom and ρ_i is the distance of each atom from the axis. For a single atom, the mass is concentrated in the nucleus, and ρ is negligible making the moment of inertia 0. For a molecule, the distance between the points of mass (atoms) and the centre of mass is sufficient enough, on the molecular level, for there to be a

significant moment of inertia and therefore a possible change in angular momentum. For a diatomic molecule, one axis will be through the centre of each atom and therefore any rotation around this axis is effectively zero on the molecular scale.

The moments of inertia of methane are equal if they describe movement in a direction at an angle of 120˚to the axis of symmetry (Herzberg 1991). Methane is therefore described as a having a symmetric top, so the moment of inertia about any axis is the same as the moment of inertia about the other two. Since all three moments of inertia are equal

$$I_A = I_B = I_C \quad [11]$$

in methane, it is known as a spherical rotor along with all molecules of the point groups T_d or O_h (Hollas 2004).

A rigid symmetric top has energy absorbed equal to

$$E = \frac{L_a^2}{2I_A} + \frac{L_b^2}{2I_B} + \frac{L_c^2}{2I_C} \quad [12]$$

where L_i is the angular momentum about each axis of rotation. The energy levels for a non-rigid spherical top are derived from the rigid term (Herzberg 1991)

$$F(J) = B(J)(J+1) \quad [13]$$

2.3 Selection Rules

Electronic transitions require much higher energies than vibrational or rotational transitions, and cannot occur in the infrared and will therefore not be discussed here. However, it is within certain electronic states that vibrational transitions occur and it is within vibrational states that rotational energy transitions occur.

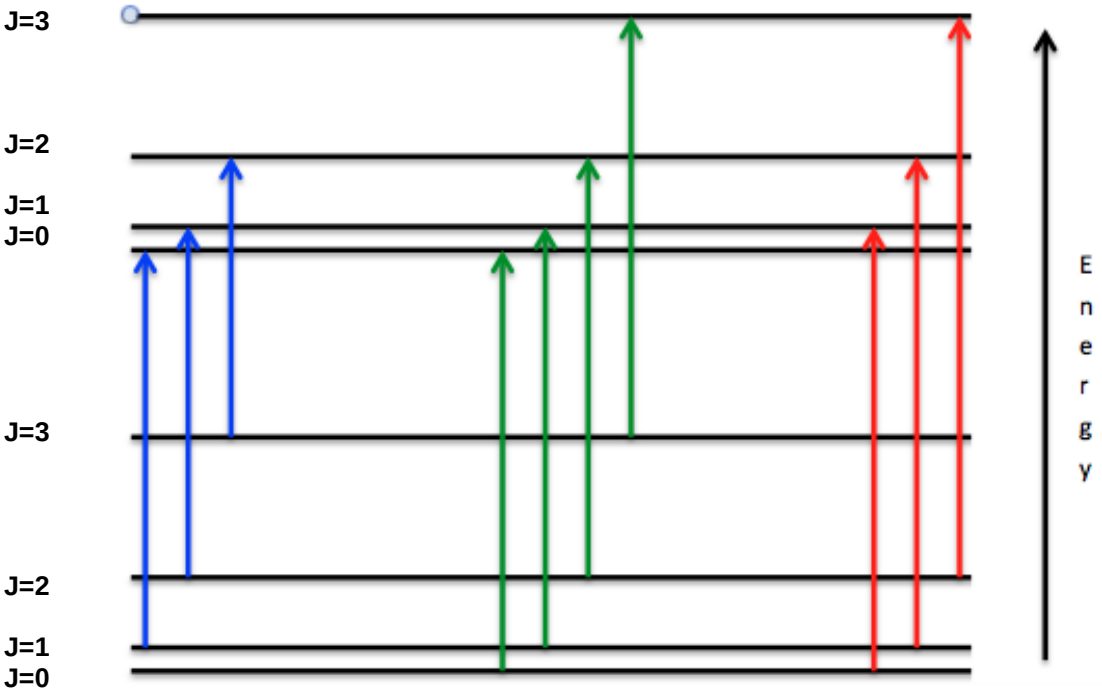

Figure 2.3: The transitions (v_0–v_1) that give rise to P (blue), Q (green) and R (red) branches

A transition is possible if the transition intensity is non-zero. For this to be the case, the following rules must be obeyed

• The molecule must have a dipole moment

• $\Delta J = 0, \pm 1$

The transitions with $\Delta J = +1$ are defined as R branches, with the transitions with $\Delta J = -1$ being defined as P branches. A $\Delta J = 0$ is allowed when multiple vibrational (also for more energetic transitions, electronic) states are involved (Figure 2.3).

2.5 Fourier Transform Spectrometry

Fourier transform spectrometry is often carried out using a system based on a Michelson interferometer, as opposed to a prism or grating in other spectrometer designs. A simple schematic of a Michelson interferometer is illustrated in Figure 2.4. A collimated source of light is split into two orthogonal beams of equal amplitude using a beam splitter. One beam will transmit in the original direction while the other will be transmitted in a direction perpendicular to that of the original direction. These beams are then reflected from mirrors at the end of each path, one of which will move and the other will remain in a fixed position, and then recombined at the beam splitter resulting in an interference pattern that may be constructive if the path difference between the two beams is zero and destructive if there is a non zero path difference. A Fourier transform then converts the inteferogram back into a spectrum, with frequencies and their associated intensities.

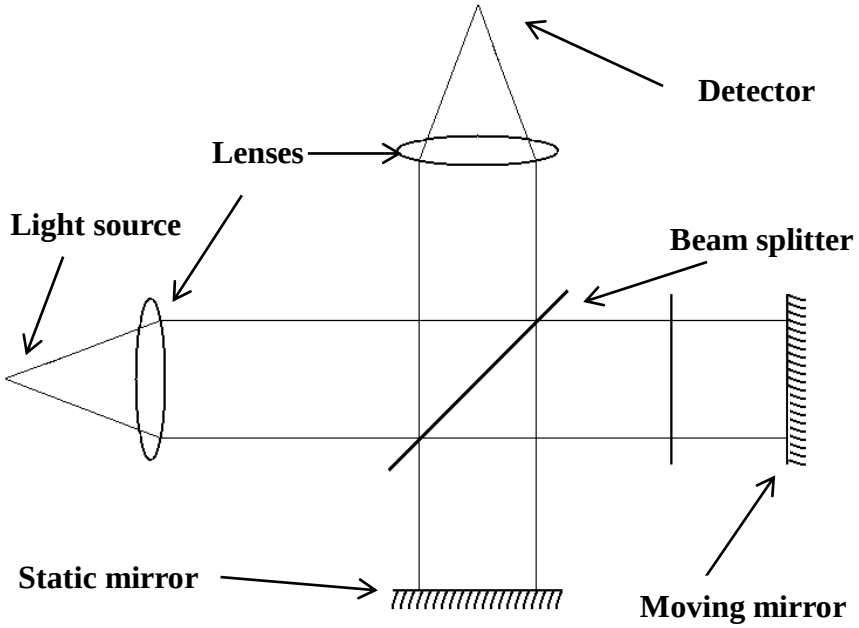

Figure 2.4: A simple representation of a Michelson interferometer.

2.5.1 Interferograms in Fourier Transform Spectrometry

The intensity of the interferogram, I(x) of a monochromatic light source is given by

$$I(x) = B(\tilde{\nu})[1 + cos(2\pi\tilde{\nu}x)] \quad [14]$$

where $B(\tilde{\nu})$ is the spectral intensity of the source as a function of wavenumber and x is the optical path difference. In reality however, the source will not be monochromatic, it will be a broadband signal, i.e. one over a broad range of frequencies and the total intensity will now be an integration over the wavenumber range

$$I(x) = \int_0^\infty B(\tilde{\nu})[1 + cos(2\pi\tilde{\nu}x)]\, d\tilde{\nu} \quad [15]$$

This is a summation of the mean intensity of the interferogram and the modulated interferogram (known as the AC component)

$$I'^{(x)} = \int_{-\infty}^{+\infty} B(\tilde{\nu})\, cos(2\pi\tilde{\nu}x)\, d\tilde{\nu} \qquad [16]$$

where the absence of negative wavenumbers gives a lower limit of -∞ for convenience. It is this modulation which is important as it is a description of the change that arises from the spectrum of the gas being investigated. The Fourier transformation of this is given by

$$B(\tilde{\nu}) = \int_{-\infty}^{+\infty} I'(x)\, cos(2\pi\tilde{\nu}x)\, dx \qquad [17]$$

where the limits of the integration are given by the maximum possible path difference, evidently this is not infinity in reality but defined by the set up of the interferometer. The integration is an idealised situation with transformation being given by the summation of discrete values determined by the sampling rate.

2.5.2 The Bruker IFS 125HR

The work outlined in this thesis was carried out using a Bruker IFS 125HR Fourier Transform Spectrometer, shown schematically in Figure 2.5. The current specification at York gives a maximum resolution of around 0.001 cm^{-1} although for obtaining spectra of hot methane, a resolution of only 0.020 cm^{-1} was required. Astronomical spectra are not

as high resolution as the spectrometer will allow. Although it may be useful for the future to have line lists at a higher resolution, given that a higher resolution requires a longer scan time and multiplied over 12 temperatures, this would make the experimental procedure more difficult and time consuming than was necessary, therefore only part of the spectrometer's path length (enough to give a 0.020 cm^{-1} resolution) was used.

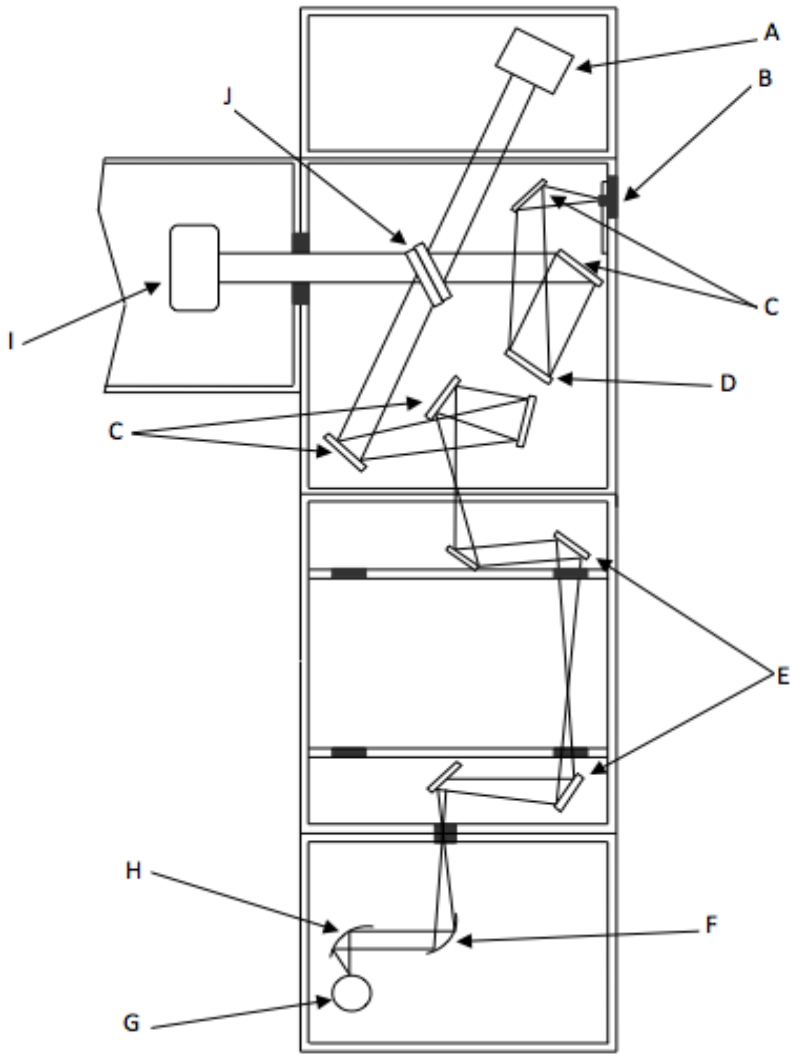

A	Fixed retroflecting mirror	F	Collimating parabolic mirror
B	Input aperture	G	Detector
C	Folding mirror	H	Focusing parabolic mirror
D	Collimating parabolic mirror	I	Scanner with movable refracting mirror
E	Toroidal mirror	J	Beam splitter

Figure 2.5: A schematic representation of the Bruker IFS 125 HR spectrometer at York. The sample is heated in a tube furnace, the radiation from which comes into the spectrometer through 'B'

References:

Bernath, P., 2005, Spectra of Atoms and Molecules (2 ed.; New York: Oxford University Press)

Herzberg, G., 1991, Molecular Spectra and Molecular Structure, Vol. II (Malabar: Krieger)

Hollas, J. M,. 2004, Modern Spectroscopy (4th ed.; Chichester: Wiley)

Rae, A. I. M,. 2002, Quantum Mechanics (New York: Taylor & Francis)

Chapter 3

Methane spectra in the infrared

3.1 Introduction

Chapter 1 of this thesis has established that in the relatively low temperatures of sub stellar objects such as brown dwarfs and exoplanets, simple molecules such as H_2O, CO, CO_2 and CH_4 may form. In order to assign these molecules in the spectra of these astronomical objects, high resolution spectra must be obtained, either theoretically, experimentally or preferably a combination of the two.

A strong methane absorption band was found in the infrared at 7.65 μm by Cushing et al. (2006) using data from the Infrared Spectroscope on board the Spitzer Space Telescope whilst observing T dwarfs and Swain et al. (2010) identified the ν_3 band P branch at 3.25 μm in the spectrum of the planet HD189733b, where observations did not match the model spectrum based on existing CH_4 line lists. However, this planet may not contain methane as this band was identified to possibly be the $2\nu_2$ band of water at 300 K (Mandel 2011). Uncertainty in the line positions of hot methane bands is evidently

limiting the assignment of observed bands in astronomical spectra. Methane is clearly prevalent in planetary atmospheres, but existing line lists such as HITRAN (Rothman et al. 2009) need to be expanded in order to improve the models which are used to explore the chemistry of the atmospheres of extrasolar planets and brown dwarfs.

Methane is a polyatomic molecule containing five atoms, a central carbon atom bonded to four hydrogen atoms, thereby having 3N – 6 = 9 fundamental modes; made up of five bending modes and four stretching modes (Bernath 2005). The bending modes are composed of a pair of ν_2 (e) modes (at 1526 cm^{-1}) and a triply degenerate bending mode, ν_4 (a t_2 bend at 1306 cm^{-1}) whereas the stretching modes are made up of a single symmetric ν_1 (a_1 at 2914 cm^{-1}) mode and a triply degenerate antisymmetric C-H stretch, ν_3 (a t_2 mode at 3020 cm^{-1}).

Although the spectra of the commonly occurring molecules, such as H_2O, NH_3 and CH_4 have been known for many years at low (296 K) temperatures, because of the hot bands and combination bands at higher temperatures that are relevant for extrasolar planets and brown dwarfs, these spectra are not wholly sufficient for a complete description of the molecule spectrum. Indeed, complete spectra at high temperatures were not known until relatively recently when ‘water on the sun’ was discovered (Wallace et al. 1995). For methane there is no complete theoretical understanding at the temperatures of cool astronomical objects (up to 4000 K) and the experimental observations are limited by limited temperature measurements that make them insufficient for modelling spectral energy distributions. Only recently have high resolution experimental data been available

for the H_2O molecule, as well as theoretical line lists (Barber et al. 2006) that in combination, can be used to analyse astronomical objects. High resolution line lists for NH_3 in the near infrared have recently been obtained by Hargreaves et al. (2011) and here we present experimental observations for methane in the region between 2.5 μm and 12.5 μm.

Currently, the best line list for methane is the HITRAN 2008 database (Rothman et al. 2009) which is generated for low temperatures and is primarily used for modelling the Earth's atmosphere. Such lists must be extrapolated for high temperatures, such as those in exoplanetary and other sub solar atmospheres, the approximate temperature range of which are 700-2000 K for brown dwarfs (Kirkpatrick 2005) and 1000-2000 K for 'hot Jupiter' extrasolar planets (Seager & Deming 2010). As such, lines from high energy transitions and hot bands are missing (Nassar & Bernath 2003) which may result in an inaccurate theoretical model. Given the relatively low temperatures of sub stellar objects compared to hydrogen burning stars, there exists a fairly rich chemical environment (Burrows 2005). Indeed, observations of these planets have shown complex spectra, with features of many commonly occurring astrophysical atoms and molecules. However, given the inaccuracy of lower temperature line lists, laboratory spectra at pertinent temperatures are required for accurate analysis of extrasolar planets.

3.2 Experimental Details

Methane spectra were recorded using a Bruker IFS 125 HR spectrometer with ZnSe and CaF_2 lenses and beamsplitters, for the lower and higher wavenumber regions respectively, and due to detector responses over the region observed, two liquid nitrogen cooled detectors namely MCT and InSb, used over the ranges 800–2200 cm^{-1} and 1800–4000 cm^{-1} respectively. The methane was heated to the desired temperature using a tube furnace to heat an Al_2O_3 tube, sealed by ZnSe or CaF_2 (depending on the region) windows at either end. The methane was then pumped through the system with a controlled flow rate to avoid impurities and loss of methane in order to keep constant sample pressure. To validate the furnace temperature reading, a thermocouple was inserted between the furnace filaments and the Al_2O_3 tube, with the assumption that the centre of the tube, which was focused on the spectrometer aperture, is at the same temperature as that of the furnace to within ±10℃. Water cooling at the ends of the tube prevented damage to the rubber O-rings in order to maintain a vacuum. This creates a cold region of methane which will absorb and reduce the intensity of the hot line spectrum. However, the CH_4 spectra obtained are reasonably assumed to be accurate to within ±10℃ of the stated temperature.

Between the lens at the end of the Al_2O_3 tube and the lens of the spectrometer, there exists gap which is filled with dry air (normal atmospheric air with water removed) in order to

reduce the water absorption lines that exist in our target region. The spectral range was chosen as it includes the 9 fundamental modes.

Spectra were taken at 100 ℃ intervals between 300 ℃ and 1400 ℃ in three sections, two with the MCT detector and one with the InSb detector with a resolution of 0.020 cm^{-1}, this was selected based on the pressure and Doppler broadening widths. The spectra between the two MCT regions were cut at 1475 cm^{-1} and between the MCT and InSb regions at 1820 cm^{-1} to result in a complete line list in the region 800-3400 cm^{-1}. The choice of cut off was made to choose the optimal signal to noise ratio for the spectrum.

Emission lines were fitted to the spectra using *WSpectra* (Carleer 2001) and a Voigt line shape profile was fitted using the same program to obtain a line list at each temperature across all three regions. Emission line amplitude inaccuracies due to the system response, a combination of the optics in the system and the sensitivities of the detectors, were corrected for by applying a black body spectrum of a graphite rod, using the method outlined in Hargreaves et al. (2011). Each line list was calibrated for wavenumber by observing the shift of identical lines from the HITRAN line lists. Unblended and symmetric lines were chosen from the experimental list and compared to those in HITRAN which were chosen for their isolation and strength. For the 1500-4000 cm^{-1} region at 1000℃, this calibration factor was 1.000001027(206) from 20 lines, where the figure in parentheses denotes the standard deviation. Similarly, the calibration factor for the 800-1450 cm^{-1} region at 1000℃ was 1.000002039(525). Across all regions and

temperatures, the calibration factors were similar to these, leading to an accuracy of the line positions in our line lists to be within ±0.002 cm^{-1}.

The intensity units in our spectra are arbitrary, so in order to provide a scale, so that they could be compared to HITRAN lists, we first converted the emission intensities into absorption intensities (Nassar & Bernath 2003) using the equation;

$$S_{absorption} = \frac{S_{emission}}{v^3 exp(-hv/kT)} \quad [18]$$

where S is the line intensity and v is the frequency at which the transition occurs. Temperature dependence of the intensity of spectral lines is described by Goldman et al. (1989). For our results, the line strength, S at a certain temperature, T can be calculated using (Nassar & Bernath 2003)

$$S = S_0 \frac{Q(T_0)}{Q(T)} exp\left(\frac{E_{low}}{kT_0} - \frac{E_{low}}{kT}\right)\left[\frac{1 - exp(-hv/kT)}{1 - exp(-hv/kT_0)}\right] \quad [19]$$

with S_0 given by the intensity of the line at the reference temperature (T_0) of 296K from HITRAN, Q(T) and Q(T_0) are the total partition functions at the measured and reference temperatures respectively. E_{low} is the lower state energy. The total partition functions are evidently temperature dependent and are a product of the vibrational partition function (Gamache et al. 2000; Herzberg 1991),

$$Q_v(T) = \prod_{i=1}^{N} \frac{1}{[1 - e^{-E_i/kT}]^{d_i}} \quad [20]$$

where E_i and d_i are the energy and the degeneracy of each of the vibrational modes at each of the four fundamental frequencies, $\tilde{\nu}_1, \tilde{\nu}_2, \tilde{\nu}_3$ and $\tilde{\nu}_4$ and the rotational partition function (Herzberg 1991);

$$\frac{Q_R(T_0)}{Q_R(T)} = \frac{\sqrt{(\pi/ABC)(kT_0/hc)^3}}{\sqrt{(\pi/ABC)(kT/hc)^3}} \quad [21]$$

for which the three rotational constants (ie quantum numbers, inversely proportional to the principle moments of inertia of the molecule) A, B and C are equal for spherical top molecules such as methane, reducing the function to equate to $(T_0/T)^{3/2}$

Table 1: Rotational, vibrational and total partition functions of methane as a ratio of experimental temperatures to HITRAN temperatures

T/C	T/K	$Q_R(T_0)/Q_R(T)$	$Q_V(T_0)/Q_V(T)$	Q_{Total}
22.85	296	1.000000000	1.000000000	1.000000000
300	573.15	0.371137742	0.857245899	0.318156308
400	673.15	0.291588097	0.765665744	0.223259017
500	773.15	0.236887381	0.667706149	0.158171161
600	873.15	0.197380516	0.571313816	0.112766216
700	973.15	0.167752069	0.481663629	0.080800070
800	1073.15	0.144859480	0.401528035	0.058165142
900	1173.15	0.126738117	0.331921070	0.042067051
1000	1273.15	0.112103250	0.272715199	0.030572260
1100	1373.15	0.100083064	0.223127705	0.022331304
1200	1473.15	0.090067293	0.182063112	0.016397932
1300	1573.15	0.081617326	0.148333591	0.012106591
1400	1673.15	0.074410676	0.120788448	0.008987950

The values in Table 1 are calculated from the values of the fundamental frequencies, 2916.5, 1533.3, 3019.49, 1306.2 cm^{-1} (Herzberg 1991b). The total partition functions are used as ratios instead of absolute values, which Nassar & Bernath (2003) found to be accurate to within 0.8% of reference values from empirical results with methane (Gamache et al. 2000) at 400 K, although this cannot be extended up to higher temperatures, but we believe this an effective method of calculating partition functions to within an acceptable degree of accuracy.

Equation (2) can therefore be used to calculate S, the line intensity.

In order to obtain the E_{low} values of the lines, we identified lines which occurred at all temperatures, plotting them with a rearrangement of Equation (19);

$$ln\frac{SQ(T)}{S_0Q(T_0)} = -\frac{E_{low}}{kT} + \frac{E_{low}}{kT_0} + ln\left[\frac{1-exp(-hv/kT)}{1-exp(-hv/kT_0)}\right] \quad [21]$$

where the lower state energy is clearly given by both the gradient and the y intercept. As such, E_{low} values can be found for each line.

3.3 Results and Analysis

Lower state energies were obtained from all three regions and combined to form one list. The ν_4 bend is clearly present in the calculated Figure 3.1. The first hot band of the Q branch at around 1300 cm^{-1} has an E_{low} of approximately 1200 cm^{-1}. A second hot band is visible at 2400 cm^{-1}.

A similar hot feature is clearer in the ν_3 mode at a slightly higher lower state energy (around 2250 cm^{-1}). The Q branch is very well defined at around 3000 cm^{-1} with P and R branches diverging from the central Q branch at approximately 1500 cm^{-1}. A second hot band is visible, but as it is broad, a single transition is not identifiable. The ν_2 mode at 1533.3 cm^{-1} is clear in the HITRAN plot, although this is not the case with our calculated lines. The Q branch is present at about 1525 cm^{-1} although it is relatively weak. An additional point of note is at 1820 cm^{-1} where the MCT and InSb detector regions were connected.

The InSb detector has a higher sensitivity and as such a break appears in the number of E_{low} produced. The P and R branches of the fundamental bands of both the ν_3 and ν_4 modes are visible down to around 1400 and 1200 cm^{-1} respectively, at which point the number of observed transitions decreases greatly. Our calculated lower state energy values are generally from transitions with high J numbers as the cooler parts of the experimental set up (Hargreaves et al. 2011) absorb the low J value fundamental lines and therefore accurate gradient values, and as such E_{low}, are less likely to be obtained.

The lower state energies across the region are shown in Figure 3.1. The hot band is visible around 3000 cm^{-1} is the $\nu_2 + \nu_3 - \nu_2$ band, forming a lower state energy of approximatetly 1500 cm^{-1}. Also contained in this is the $\nu_2 + \nu_1 - \nu_2$ band. There also looks to be the origins of an even hotter band, which is not so well defined. An R-branch can also be seen from the fundamental ν_3 and ν_1 bandsnear 3200 cm^{-1}.

At 1300 cm^{-1} the clearest band is the $2\nu_4 - \nu_4$ band. The $3\nu_4 - 2\nu_4$ band is also visible at a higher lower state energy. The R branch of the ν_4 fundamental is clearly visible.

In addition to observed lines we have added HITRAN (2008) lines into our line list (Figure 3.2). In our experiment strong emission lines may be self-absorbed, so matching lines are better represented by HITRAN values extrapolated for temperature. The lines that were observed experimentally that also exist in HITRAN (above 1×10^{-22} cm/molecule) were replaced by the corresponding HITRAN value. Table 2 shows the number of observed lines and HITRAN lines for each temperature.

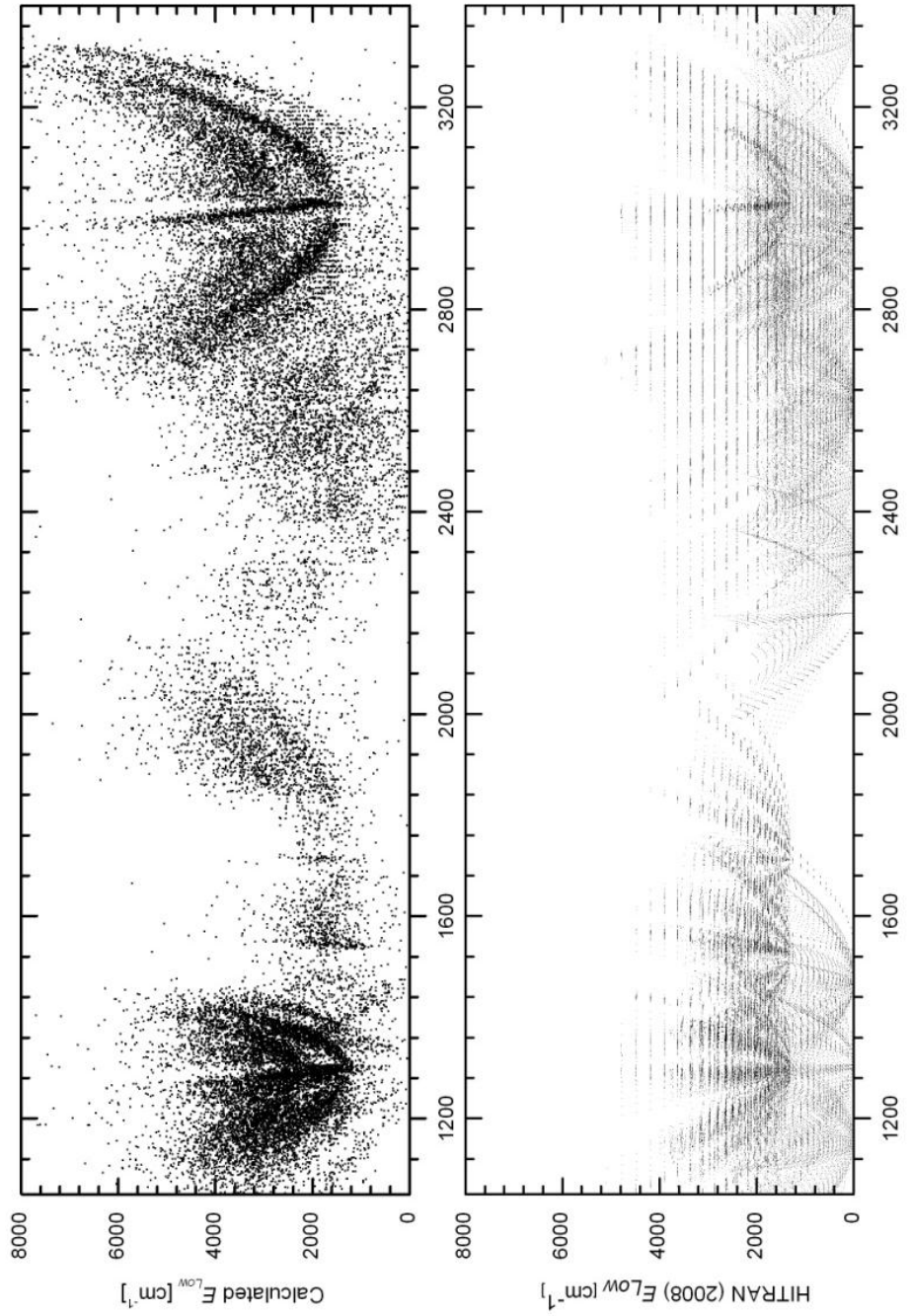

Figure 3.1: Lower state energy values for experimental lines (top) and HITRAN (2008) lines, (bottom) from 1000 to 3400 cm^{-1}

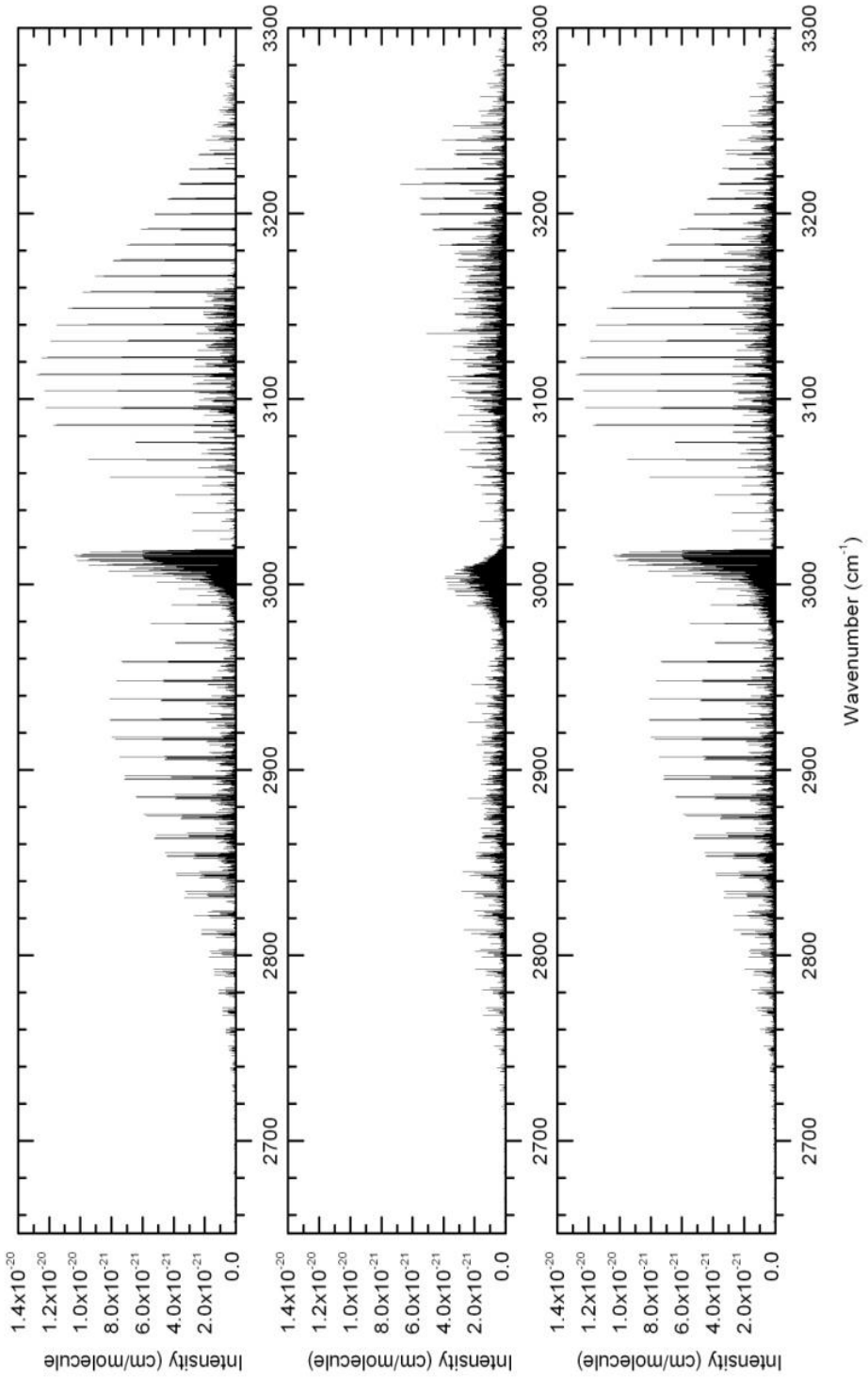

Figure 3.2: Extrapolated HITRAN lines (top), experimental lines (middle) and combined HITRAN and experimental lines (bottom)

Table 2. The number of lines present in each line list, by temperature and line type.

Temperature (˚C)	Total Lines	Observed lines	Added HITRAN Lines
300	21427	2315	19112
400	27589	5967	21622
500	30577	7602	22975
600	37754	14508	23246
700	38570	15681	22889
800	43770	21564	22206
900	47016	25591	21425
1000	46893	27414	19479
1100	44570	26349	18221
1200	45521	28522	16999
1300	45435	29738	15697
1400	28145	13819	14326

The most accurate values for the lower state energies are given when the gradient from Equation (21) is calculated from the lines of 10 or more spectra. These are given a 'quality identifier' of 1. E_{low} values calculated from less than 10 spectra, but from at least 3 spectra below 1000^{o}C are given the quality identifier of 2 and E_{low} values that are calculable from any three spectra regardless of temperature are given a quality identifier of 3. Where no lower state energy can be accurately determined a quality identifier of 0 is used. Added HITRAN lines are given an identifier of '1H'.

Table 3. A sample line list of 10 lines from the 900°C list

Wavenumber (cm^{-1})	Intensity (cm/molecule)	E_{Low} (cm^{-1})	Quality Identifier
...	...	...	...
1745.9202881	1.09E-22	0.00E+00	0
1746.6003418	1.19E-22	2.98E+03	2
1746.8721924	9.46E-23	1.73E+03	2
1746.8756104	9.46E-23	1.86E+03	3
1748.0861816	1.11E-22	1.33E+03	1
1752.0727539	5.31E-23	1.08E+03	2
1752.1606445	8.84E-23	3.24E+03	2
1752.1627197	8.84E-23	1.58E+03	3
1752.4083400	1.25E-22	1.56E+03	1H
1752.4083400	1.25E-22	1.56E+03	1H
...	...	...	...

3.4 Discussion of results

We have produced line lists for methane, intensity calibrated to HITRAN values extrapolated for temperature (Equation 19). We also claim a wavenumber calibration compared to HITRAN to be within 0.002 cm^{-1}. The intensity calibration can be corrupted by mismatched lines and as such, a large number of calibration lines were used in order to minimise the effect of mismatched lines. The temperature of the center of the Al_2O_3 tube is accurate to within ±10 K, however, at the ends of the tube, the temperature is much lower. There is also an air gap between the spectrometer and the furnace tube. Although the general absorption peaks can be accounted for in the analysis of the spectra, they are indicative of the problems faced with the method. The temperature gradient, along with the constant heating of the tube, mean that during the time of the scan the temperature is not constant, but in fact it varies over a small range. The spectra are therefore measurements of the emission lines over a distribution of temperatures. Small absorption peaks created by the presence of water in the air gap can create broad absorption bands in which methane emission lines can exist, as such, the strengths of these lines are difficult to quantify precisely. This effect is also noticeable at low temperatures and outside of the main bands, where the signal to noise ratio will clearly be lower. Line fitting in polyatomic molecules is difficult, and WSpectra can incorrectly assign a peak of a blended line, or even the ‘shoulder’ of a peak, and this error cannot be accounted for without correct assignment of every line. An incorrect assignment makes

comparison with HITRAN difficult as there may not be a line at that position, or it may wrongly match lines of different strengths. Intensity calibration is therefore potentially obscured in methane and as such these may result in errors in the empirical lower state energies. The matching is also affected by emission along the gradient between the cool ends of the tube where absorption occurs and the hot center. The emission at these points creates lines that are weaker, but at the correct line position. However at cooler temperatures, this effect is reduced due to the lesser photon flux resulting from these thermal energies.

The detector responses have been accounted for by taking a black body spectrum and the recorded intensities were corrected by applying the response function of the instrument. The largest corrections are at either side of each region and therefore the overlaps of the regions were chosen in part, so as to minimize large corrections due to the instrument response function. The intensity calibration factors were obtained from the ratios between HITRAN lines and our experimentally obtained lines. This is notoriously difficult and is the main source of error in our line lists. Outliers from these ratios were discarded and classified as mismatched lines. However, within ratios deemed to be from matches, the values differed by up to 30% and the ratio used were selected to be around the mean of these, whilst recognizing that the final intensities of overlapping regions should be similar.

Our data can be used to validate ab initio models of methane which use an extrapolation of lower temperature values. Both experimental and theoretical methods for obtaining

high temperature line lists are important and both have their strengths and weaknesses. Low intensity lines are difficult to distinguish experimentally and we found lines which were apparent at hot temperatures, but the signal to noise ratio at colder temperatures made ascertaining the intensity of the peak impossible. Theoretical models to assign these low intensity lines would be useful and could corroborate our results for a more complete analysis of methane in our spectral region at 'hot' temperatures.

References:

Barber R. J., Tennyson J., Harris G. J., Tolcehenov R., 2006, MNRAS, 368, 1087

Bowler, B. P., et al., 2010, Astrophysical Journal, 723, 850

Burrows, A., 2005, Nature, 433, 261

Carleer, M. R., 2001, Proc. SPIE, 4168, 377

Charbonneau, D., et al., 2000, Astrophysical Journal, 529, L45

Charbonneau, D., et al., 2002, Astrophysical Journal, 568, 377

Courtin, R., Gautier, D., Marten, A., & Bezard, B., 1984, Astrophysical Journal, 287, 899

Fortman, S. M., et al. 2010, Astrophysical Journal, 714, 476

Gamache, R. R., Kennedy, S., Hawkins, R., & Rothman, L. S. 2000, Journal of Molecular Structure, 517, 407

Goldman, A., Dang-Nhu, M., Bouanich, J. P., 1989, JQSRT, 41, 17

Hargreaves, R. J., Li, G., Bernath, P. F., 2011, Astrophysical Journal, 735, 111

Herzberg, G., 1991, Molecular Spectra and Molecular Structure, Vol. II (Malabar: Krieger)

Herzberg, G., 1991, Molecular Spectra and Molecular Structure, Vol. III (Malabar: Krieger)

Henry, G. W., et al. 2000, Astrophysical Journal, 529, L41

Kirkpatrick, J. D. 2005, ARAA, 43, 195

Mandell, A. M., et al. 2011, Astrophysical Journal, 728, 18

Nassar, R., & Bernath, P. 2003, JQSRT, 82, 279

Redfield, S., et al., 2007, Astrophysical Journal, 673, L87

Rothman, L. S. et al.2009, JQSRT., 110, 533

Seager, S., 2008, Space Science Review, 135, 345

Seager, S. & Deming, L. D. 2010, ARAA., 48, 631

Snellen, I. A. et al., 2008, Astronomy & Astrophysics, 487, 357

Swain, M. R. et al. 2009, Astrophysical Journal, 704, 1616

Swain, M. R., et al. 2010, Nature, 463, 637

Tinetti, G., et al. 2007, Nature, 448, 169

Chapter 4

Conclusions and Further Work

Line lists have been obtained using high resolution Fourier transform spectroscopy at 12 temperatures between 300 and 1400 ^{o}C at 100 ^{o}C intervals. This temperature range is pertinent due to the fact that existing line lists such as HITRAN are at room temperature. Such cold temperatures do not fully represent the temperature regimes in many exoplanets and brown dwarf atmospheres for example as hot bands may be missed. It is important when modeling spectra to analyse observed spectra from astronomical sources to include all possible lines. Modelers are greatly assisted by the inclusion of lower state energies, which we present as part of the line lists. This line list, including the lower state energies will be used to calculate model spectra. The spectra were taken in the spectral region 800-3400 cm^{-1} which is in the spectral range of many land and space based observatories studying exoplanets and brown dwarfs. This work was driven by application and in both temperature and spectral ranges; the results assist modelers in the

growing science of astronomical atmosphere study. Given the pertinence of the spectral region observed and the calculation of lower state energies, this line list will be extremely useful in the prediction of spectra of the atmospheres of substellar objects which can then be compared to astronomically observed spectra in order to ascertain the chemical composition of such an object.

To date, line lists have been compiled for a select number of molecules. However, there are still many molecules that are found in planetary atmospheres that do not have a complete experimentally produced line list or a full theoretical understanding. Both must be pursued in order to make the models of spectra as accurate as possible. An extension of the target spectral regions is also beneficial and work is currently being undertaken in order to analyse the spectrum of methane and ammonia up to 7000 cm^{-1}.